Selective catalytic reduction of nitric oxide with a novel Mn–Ti–Ce oxide core-shell catalyst having improved low-temperature activity and water tolerance

Li, Huirong; Schill, Leonhard; Fehrmann, Rasmus; Riisager, Anders

Published in:
Journal of the Energy Institute

Link to article, DOI:
10.1016/j.joei.2023.101266

Publication date:
2023

Document Version
Publisher's PDF, also known as Version of record

Journal of the Energy Institute 109 (2023) 101266

Contents lists available at ScienceDirect

Journal of the Energy Institute

journal homepage: www.elsevier.com/locate/joei

Selective catalytic reduction of nitric oxide with a novel Mn–Ti–Ce oxide core-shell catalyst having improved low-temperature activity and water tolerance

Huirong Li, Leonhard Schill, Rasmus Fehrmann, Anders Riisager *

Centre for Catalysis and Sustainable Chemistry, Department of Chemistry, Technical University of Denmark, 2800, Kgs. Lyngby, Denmark

ARTICLE INFO

Handling Editor: Paul Williams

Keywords:
Multi-shell structure
Selective catalytic reduction
NO_x removal
Redox property
Surface acidity

ABSTRACT

A novel core-shell-shell Mn–Ti–Ce oxide catalyst (MnO_x@TiO_2@CeO_2) was synthesized by a three-step method and applied for the selective catalytic reduction of NO_x with ammonia (NH_3-SCR). The catalyst exhibited an excellent low-temperature activity with NO_x conversion >80% in a broad temperature range under both dry (120–260 °C) and wet (180–255 °C) conditions with a weight hourly space velocity (WHSV) of 240,000 mL/(g·h). Nitrogen physisorption and X-ray photoelectron spectroscopy (XPS) results showed that the formation of the inner TiO_2 shell significantly increased the specific surface area, surface Mn^{4+}/Mn ratio and chemisorbed oxygen, which could provide more active sites and promote the oxidation of NO to NO_2. Ammonia temperature-programmed desorption (NH_3-TPD) results indicated that the formation of the outer CeO_2 shell not only extensively increased the surface acid sites but also enhanced the acid strength, beneficial for the ammonia adsorption and resulting in a good water tolerance.

1. Introduction

The combustion of fuels in stationary and mobile units forms flue gases containing nitrogen oxides (NO_x, mainly NO and NO_2), which upon emission to the atmosphere induce acid rain, photochemical smog and haze endangering the environment and human health [1,2]. To mitigate such NO_x emissions several technologies have in the last decades been developed of which the selective catalytic reduction of NO_x with NH_3 (NH_3-SCR) is the most effective and most widely used deNO_x technology [3–6].

Industrially applied NH_3-SCR catalysts are typically based on vanadia-tungsta (or molybdena) supported on titania, i.e. V_2O_5-WO_3(MoO_3)/TiO_2 (VWT catalysts). VWT catalysts exhibit high N_2 selectivity and good thermal stability [7–9]. However, a required operating temperature of 300–400 °C makes it necessary to locate the catalysts upstream of any dust removal and/or desulfurization in order to avoid reheating of the flue gas. This makes VWT catalysts prone to deactivation or inhibition by impurities in the flue gas such as, e.g. SO_2, alkali- or heavy metals. Additionally, the toxic vanadium inventory possesses a concern with respect to disposal of discarded catalysts [10–12].

Mn-based catalysts exhibit much higher low temperature (LT) NH_3-SCR activity than V-based catalysts and are thus attractive low cost and environmentally benign alternatives to VWT catalysts [13–16]. Nevertheless, pure MnO_x catalysts suffer from narrow active temperature window, poor N_2 selectivity at higher temperatures (>200 °C) and high sensitivity to H_2O and SO_2. Extensive work by doping with other transition/rare earth metals (e.g., Ce, Ni, Fe and Co) [17–19], or application of different support materials (e.g., TiO_2, Al_2O_3 and titania nanotubes) [20–23] has proven to significantly improve the N_2 selectivity of pure MnO_x catalysts [13,24,25], but the poor resistance to H_2O and SO_2 remains a great challenge for practical applications [26].

Core-shell catalysts (usually written as core@shell) contain an inner catalytically active core with one or more outer shells [27–29]. The core@shell assembly can induce superior material properties compared to the individual shell and core materials as well as prevent migration of the core and protect it from poisoning [30,31]. Using this methodology, Sheng et al. [32] prepared a NH_3-SCR MnO_x@TiO_2 catalyst by a two-step method, which exhibited high activity, high stability, excellent N_2 selectivity as well as better SO_2 and H_2O resistance compared to a traditional supported MnO_x/TiO_2 catalyst. The improved SO_2 resistance was attributed to the evenly distributed TiO_2 shell preserving more Mn^{4+} active centers in MnO_x@TiO_2 after poisoning. Likewise, Huang et al. [33] have prepared a $MnFeO_x$@TiO_2 catalyst by dipping deposition

* Corresponding author.
E-mail address: ar@kemi.dtu.dk (A. Riisager).

https://doi.org/10.1016/j.joei.2023.101266
Received 18 January 2023; Received in revised form 3 May 2023; Accepted 9 May 2023
Available online 9 May 2023

that exhibited higher K resistance than a $MnFeO_x/TiO_2$ catalyst prepared by impregnation method, due to the protective effect of the TiO_2 shell on the core species. On the other hand, Yu et al. [34] introduced a novel MnO_x@Eu-CeO_x nanorod catalyst with multiple protective attributes using a chemical precipitation method. The MnO_x@Eu-CeO_x catalyst exhibited superior SCR performance and strong SO_2 tolerance due to enhanced surface acidity and redox properties, which also reduced the deposition of surface sulfates. Oppositely, Huang et al. [35] prepared and introduced a core-shell-shell Ce@Mn@TiO_x catalyst with high redox capacity due to the co-existence of Ce and Mn and high surface acidity due to coating of the outer TiO_2 shell. The high acidity promoted the adsorption and activation of NH_3 resulting in excellent LT catalytic performance as well as wide working temperature window. Notably, the TiO_2 shell also protected the active sites from competitive adsorption of H_2O and SO_2 leading to better resistance of the components.

In this work, a series of MnO_x nanorods and derived novel core-shell catalysts with TiO_2 and CeO_2 were prepared and systematically evaluated with respect to catalytic activity and H_2O resistance for LT NH_3-SCR. Various methods of characterization were applied to investigate the core-shell nanostructures and the physicochemical properties of the catalysts in order to correlate material characteristics and catalytic performance.

2. Experimental

2.1. Catalyst preparation

2.1.1. MnO_x catalyst

MnO_x nanorods were prepared via a traditional hydrothermal method using the following protocol: A solution of 2.50 g (15 mmol) $KMnO_4$ (≥99.0%, Sigma) and 1.00 g (5 mmol) $MnSO_4{\cdot}H_2O$ (≥99.0%, Sigma) in 100 mL of deionized water was stirred (500 rpm) at room temperature for 1 h, and then transferred to an autoclave with Teflon inset for thermal treatment at 140 °C for 12 h. After reaction, the autoclave was cooled to room temperature and the resulting product collected and washed thoroughly (6 × 250 mL) with deionized water by intermediate centrifugation (12,000 rpm, 10 min), dried at 100 °C overnight, and finally calcined in air at 500 °C for 2 h (heating rate 2 °C/min).

2.1.2. MnO_x@TiO_2 catalyst

A core-shell MnO_x@TiO_2 catalyst was synthesized by a kinetics-controlled coating method using the synthesized MnO_x nanorods [36]. 0.176 g (~2.00 mmol) MnO_x nanorods (uncalcined) was dispersed in 100 mL abs. ethanol (≥99.8%, VWR), whereafter 0.4 mL 25 wt% aq. ammonia (p.a., VWR) was added to the solution followed by ultrasonication for 30 min. Afterwards, 0.75 mL (2.00 mmol) tetrabutyl titanate (97.0%, Sigma) was added dropwise to the solution and the mixture maintained at 45 °C for 24 h under continuous magnetic stirring (500 rpm). After cooling to room temperature, the final product was collected and washed thoroughly (6 × 250 mL) with deionized water by intermediate centrifugation (12,000 rpm, 10 min), dried at 100 °C overnight and finally calcined in air at 500 °C for 2 h (heating rate 2 °C/min).

2.1.3. MnO_x@TiO_2@CeO_2 catalysts

Core-shell-shell MnO_x@TiO_2@CeO_2 catalysts were synthesized by a self-assembly method using synthesized MnO_x@TiO_2 catalyst. 0.179 g (~1.00 mmol) MnO_x@TiO_2 (uncalcined) was dispersed in a mixture of 40 mL deionized water and 40 mL abs. ethanol followed by adding first 0.108 g (0.25 mmol) $Ce(NO_3)_3{\cdot}6H_2O$ (≥99.0%, Sigma) and then 0.070 g (0.50 mmol) hexamethylenetetramine (HMT) (≥99.0%, Sigma). After stirring at room temperature for 30 min, the mixture was heated to 75 °C and refluxed for 2 h with stirring (500 rpm). The resulting precipitate was collected and washed thoroughly (6 × 250 mL) with deionized water by intermediate centrifugation (12,000 rpm, 10 min), dried at 100 °C overnight and finally calcined in air at 500 °C for 2 h (heating rate 2 °C/min).

The prepared catalyst was denoted MnO_x@TiO_2@CeO_2-0.25, where 0.25 refers to the theoretical molar ratio of Ce/Mn. Three analogous catalysts with different Ce/Mn ratios were synthesized by the same method as above, and denoted MnO_x@TiO_2@CeO_2-0.5 (Ce/Mn = 0.50), MnO_x@TiO_2@CeO_2-0.75 (Ce/Mn = 0.75) and MnO_x@TiO_2@CeO_2-1.0 (Ce/Mn = 1.0), respectively.

2.1.4. MnO_x@CeO_2 catalysts

Core-shell MnO_x@CeO_2 catalysts with molar Ce/Mn ratios of 0.25, 0.50, 0.75 and 1.0 were synthesized by the self-assembly method described for MnO_x@TiO_2@CeO_2 and denoted in a similar way as MnO_x@CeO_2-0.25, MnO_x@CeO_2-0.5, MnO_x@CeO_2-0.75 and MnO_x@CeO_2-1.0, respectively.

2.1.5. MnO_x@CeO_2@TiO_2 catalyst

A core-shell-shell MnO_x@CeO_2@TiO_2-0.5 catalyst was synthesized from the pre-obtained MnO_x@CeO_2-0.5 catalyst by a kinetics-controlled coating method analogously to the procedure described for the preparation of MnO_x@TiO_2.

2.2. Catalyst characterization

X-ray powder diffraction (XRD) measurements were carried out on a Huber G670 powder diffractometer using Cu Kα radiation within a 2θ range of 5–85°.

Transmission electron microscopy (TEM) and elemental mapping by energy-dispersive X-ray spectroscopy (EDS) were recorded on a Tecnai T20 electron microscope equipped with Oxford EDS detector (X-Max 80 T) and an acceleration voltage of 200 kV.

Nitrogen adsorption-desorption isotherms were measured on a Micromeritics ASAP 2010 instrument at −196 °C. Prior to each test, the sample was degassed at 300 °C for 3 h.

X-ray fluorescence (XRF) was measured on an Epsilon 3 spectrometer (PANalytical B.V., Almelo). Before measurement, 0.1 g of the sample was mixed with 10.4 g flux (67% $Li_2B_4O_7$, 33% $LiBO_2$) and then heated to 1050 °C in a Claisse LeNeo Fusion Oven to obtain a fused bead.

X-ray photoelectron spectroscopy (XPS) was performed ex-situ with a Thermo Scientific system at room temperature using Al Kα radiation (1484.6 eV) and a spot size of 400 μm. A flood gun was used to reduce sample charging effects. Data processing was done using the Avantage 5.948 software and all binding energies were before deconvolution calibrated relative to the C 1s (284.8 eV).

Thermogravimetric analysis (TGA) was conducted on a Mettler Toledo TGA/DSC 1 SF instrument. About 8 mg of sample was placed in a 70 μL alumina crucible and heated from room temperature to 800 °C at a rate of 10 °C/min in N_2 flow (20 mL/min).

Temperature-programmed desorption of NH_3 (NH_3-TPD) was conducted on a Micromeritics Autochem-II instrument equipped with a thermal conductivity detector (TCD). 100 mg of the sample was prior to a typical measurement treated in He flow (50 mL/min) at 300 °C for 1 h and cooled to 100 °C. Then the sample was exposed to 1% NH_3/He (50 mL/min) for 1 h, followed by purging with He (50 mL/min) at 100 °C for 30 min to remove weakly adsorbed NH_3. Finally, the sample was heated to 600 °C at a rate of 10 °C/min in He flow (50 mL/min) and the desorbed NH_3 quantified with the TCD detector.

Temperature-programmed reduction of H_2 (H_2-TPR) was performed on the same instrument as NH_3-TPD. Prior to a typical measurement, 50 mg sample was treated in He flow (50 mL/min) at 300 °C for 1 h and cooled to 50 °C. Then, the sample was heated to 800 °C at a rate of 10 °C/min in 5% H_2/Ar flow (50 mL/min), while H_2 consumption was quantified with the TCD detector.

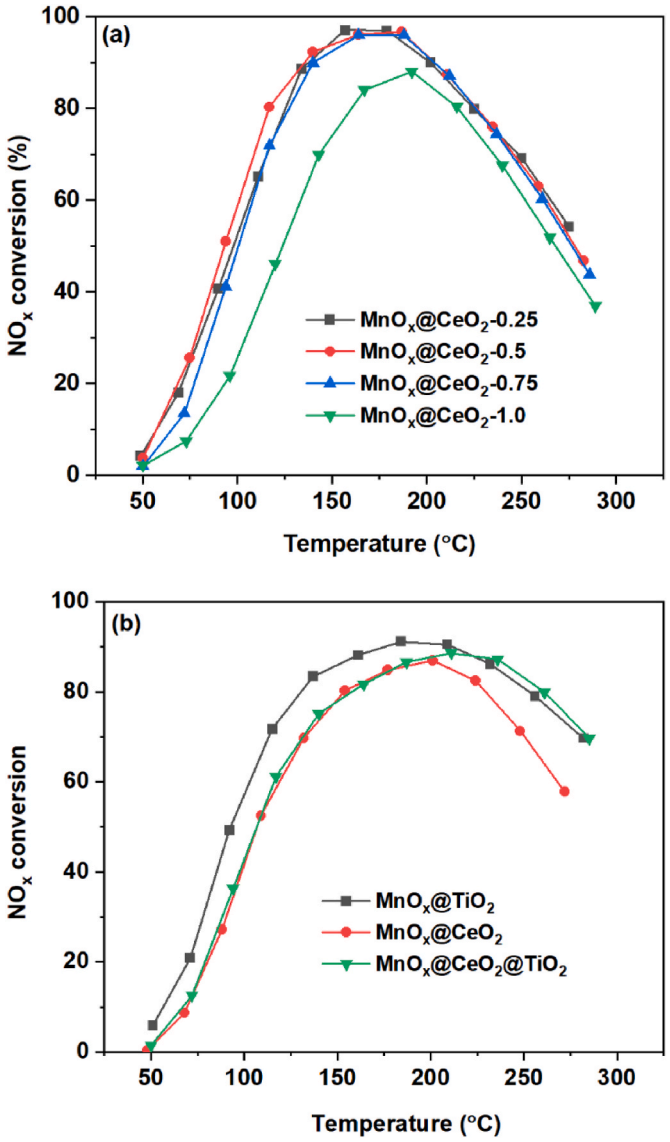

Fig. 1. NO_x conversion of (a) MnO_x@CeO_2 catalysts with different Ce/Mn ratios (WHSV = 120,000 mL/(g·h)) and (b) MnO_x@TiO_2, MnO_x@CeO_2 and MnO_x@CeO_2@TiO_2 catalysts (WHSV = 240,000 mL/(g·h)). Reaction conditions: [NO] = [NH_3] = 600 ppm, [O_2] = 4.5 vol%, balanced by N_2.

2.3. Catalytic activity test

The NH_3-SCR activity tests were done with 50 mg of fractionized catalyst (0.25–0.355 mm) in a fixed-bed quartz reactor (inner diameter 3.74 mm) using a feed gas containing 600 ppm NO, 600 ppm NH_3, 4.5 vol% O_2, 2.5 or 10 vol% H_2O (when used) and N_2 as the balance. The total gas flow rate was either 100 or 200 mL/min corresponding to a weight hourly space velocity (WHSV) of 120,000 or 240,000 mL/(g·h), respectively. The concentration of the effluent gases NO, NO_2 and NH_3 from the reactor was continuously monitored using a 17C NH_3 Analyzer (Thermo Electron Corporation) after reaching a steady state at each reaction temperature.

The NO_x conversion (X) was calculated as Eq. (1), where $C_{NOx,in}$ and $C_{NOx,out}$ are the inlet and outlet concentrations of gaseous NO_x, including both NO and NO_2.

$$X = \frac{C_{NO_x,in} - C_{NO_x,out}}{C_{NO_x,in}} \times 100\ \% \quad (1)$$

The rate constants (k) were derived from NO_x conversion measured under steady state and calculated as shown in Eq. (2) assuming a first-order reaction of NO and plug flow conditions, where F is the total molar flow rate (mol/s), W is the mass of catalyst (g), and X is the NO_x conversion (%).

$$k = -\frac{F}{W}\ln(1 - X) \quad (2)$$

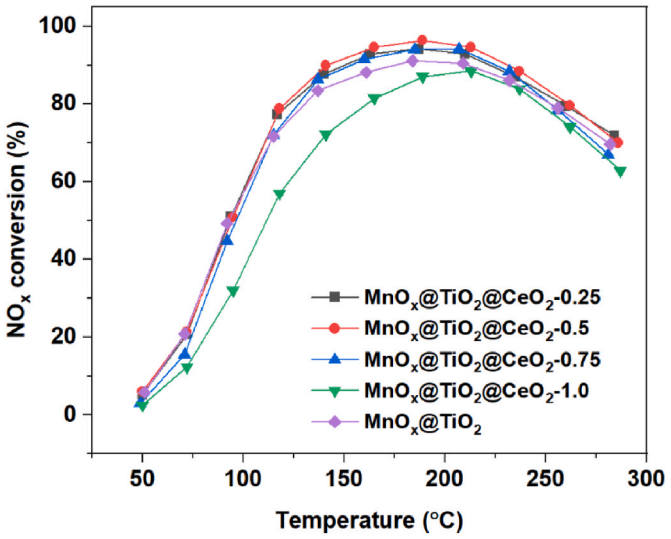

Fig. 2. NO_x conversion of MnO_x@TiO_2@CeO_2 catalysts with different Ce/Mn ratios. Reaction conditions: [NO] = [NH_3] = 600 ppm, [O_2] = 4.5 vol%, balanced by N_2, WHSV = 240,000 mL/(g·h).

3. Results and discussion

3.1. NH_3-SCR activity of catalysts

The NH_3-SCR performance (i.e. NO_x conversion) of the prepared MnO_x@CeO_2 catalysts with different Ce/Mn ratios were initially measured in the temperature range 50–280 °C (Fig. 1a). The MnO_x@CeO_2-0.5 catalyst (denoted as MnO_x@CeO_2 in the following) exhibited slightly better LT performance (<150 °C) than the catalysts with alternative Ce/Mn ratios and was therefore used a basis for the synthesis of the core@shell@shell catalyst MnO_x@CeO_2@TiO_2. This double-layered catalyst exhibited lower LT SCR activity compared to the mono-layered MnO_x@TiO_2 catalyst, but similar activity as MnO_x@CeO_2 catalyst at low temperatures (<200 °C) (Fig. 1b). Oppositely, the SCR activity of the MnO_x@CeO_2@TiO_2 catalyst was superior at higher temperatures (>225 °C), suggesting that the outer TiO_2 shell diminished the undesired oxidation of NH_3 to NO.

A series of alternative MnO_x@TiO_2@CeO_2 catalysts with different Ce/Mn ratios were tested next (Fig. 2). Overall, the activity trends of the MnO_x@TiO_2@CeO_2 catalysts were the same as for the MnO_x@CeO_2 catalysts with the catalyst having Ce/Mn ratio of 0.5, i.e. MnO_x@TiO_2@CeO_2-0.5 (denoted as MnO_x@TiO_2@CeO_2 in the following) performing the best at all temperatures 50–280 °C. Notably, the obtained NO_x conversion of 96% at 185 °C with relatively high WHSV was superior performance compared to Mn-based catalysts previously reported in literature (Table S1), and the corresponding reaction rate constant (k) of MnO_x@TiO_2@CeO_2 at 100 °C was accordingly also much higher than the alternative catalysts. At lower WHSV (60,000 and 120,000 mL/(g·h)) most catalysts reached a plateau with full NO_x conversion in a broad temperature range from already 100 °C (Fig. S1), thus making it difficult to distinguish their performance. Therefore, the higher WHSV of 240,000 mL/(g·h) was applied for further study and comparison.

A more detailed analysis of the activity profiles of the MnO_x@TiO_2@CeO_2 catalyst and the MnO_x and MnO_x@TiO_2 catalysts with dry

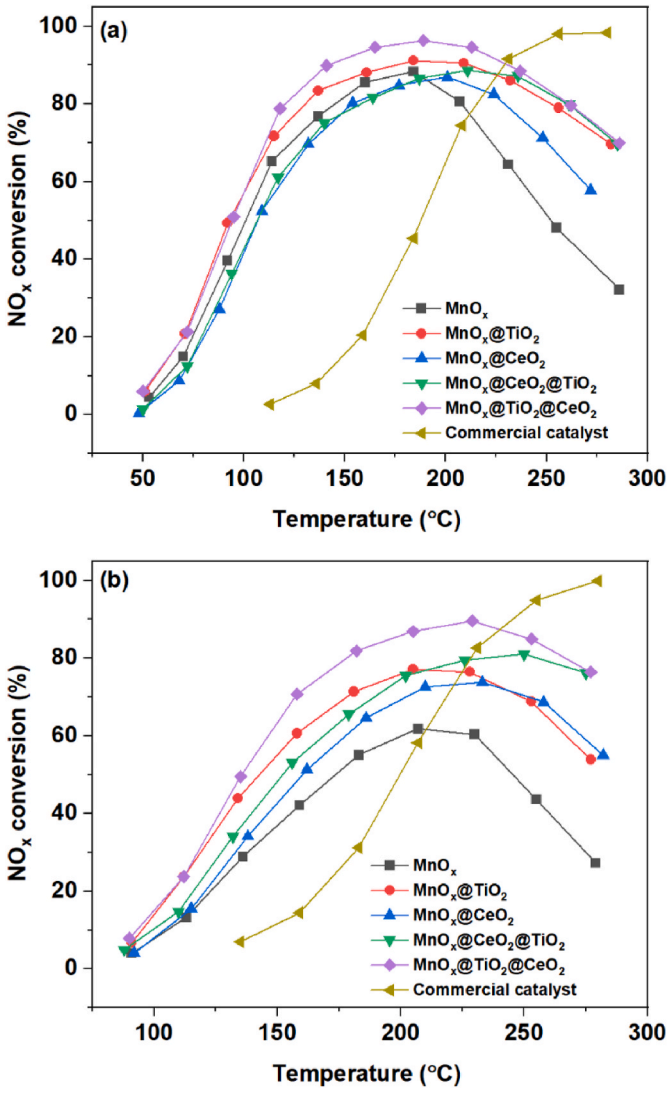

Fig. 3. NO_x conversion of MnO_x, $MnO_x@TiO_2$, $MnO_x@CeO_2$, $MnO_x@CeO_2@TiO_2$, $MnO_x@TiO_2@CeO_2$ and commercial VWT catalyst (3 wt% V_2O_5-7 wt.% WO_3/TiO_2) (a) without water and (b) with water in the feed gas. Reaction conditions: [NO] = [NH_3] = 600 ppm, [O_2] = 4.5 vol%, [H_2O] = 2.5 vol% (when used), balanced by N_2, WHSV = 240,000 mL/(g·h).

feed gas (Fig. 3a), revealed that the temperature window with NO_x conversion >80% (T_{80}) broadened gradually when MnO_x was coated with the TiO_2 shell to $MnO_x@TiO_2$ (135–250 °C) and with an additional outer shell of CeO_2 to $MnO_x@TiO_2@CeO_2$ (120–260 °C). Moreover, $MnO_x@TiO_2@CeO_2$ showed significantly higher LT (<200 °C) activity than a commercial VWT (3 wt% V_2O_5-7 wt.% WO_3/TiO_2) catalyst. In addition, $MnO_x@TiO_2@CeO_2$ exhibited a good stability at 185 °C (Fig. S2). Based on k values calculated by Eq. (2) for $X < 50\%$, the Arrhenius plots of MnO_x and MnO_x-derived catalysts in the temperature range 50–100 °C and the commercial VWT catalyst in the temperature range 115–185 °C (Fig. S3) showed also that $MnO_x@TiO_2@CeO_2$ had the lowest apparent activation energy (E_a) of 53.6 kJ/mol conducive for the NH_3-SCR reaction.

In the presence of water in the gas feed (2.5 vol%), the catalytic activity of the pure MnO_x catalyst was significantly inhibited by the water vapor whereas the core-shell catalysts showed much better H_2O tolerance. Especially $MnO_x@TiO_2@CeO_2$ maintained a high NO_x conversion with T_{80} in the temperature range 180–255 °C (Fig. 3b). Similarly, the $MnO_x@TiO_2@CeO_2$ catalyst was also much less effected when exposed to a feed gas with a higher water concentration (10 vol%) for 2

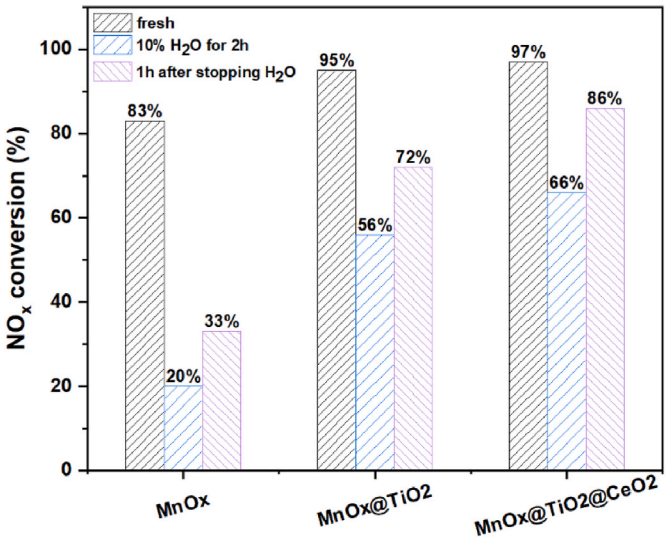

Fig. 4. Water resistance tests of MnO_x, $MnO_x@TiO_2$ and $MnO_x@TiO_2@CeO_2$ at 185 °C. Reaction conditions: [NO] = [NH_3] = 600 ppm, [O_2] = 4.5 vol%, [H_2O] = 10 vol% (when used), balanced by N_2, WHSV = 240,000 mL/(g·h).

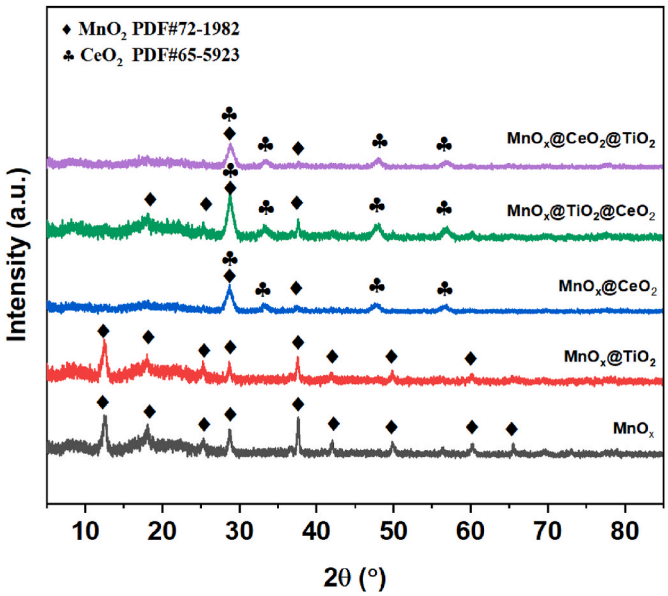

Fig. 5. XRD patterns of MnO_x and derived core-shell catalysts.

h at 185 °C (Fig. 4). Importantly, the catalyst recovered also significantly more of its original activity (86%) after 1 h of re-exposure to dry feed gas in comparison to the MnO_x (38%) and $MnO_x@TiO_2$ (72%) catalysts. Hence, overall the encapsulated MnO_x core with an inner shell of TiO_2 and an outer shell of CeO_2 improved both the NH_3-SCR activity as well as water resistance.

3.2. Characterization of catalysts

3.2.1. Structure, morphology and porosity

XRD was used to determine the phase compositions of MnO_x and the derived core-shell catalysts (Fig. 5). Only characteristic peaks of crystalline MnO_2 (JCPDS PDF 72–1982) were detected in the diffraction patterns of MnO_x and $MnO_x@TiO_2$, indicating a high dispersion of TiO_2 in the latter catalyst which was further confirmed by the elemental mapping (Fig. S4). For $MnO_x@TiO_2@CeO_2$ new diffraction peaks appeared corresponding to CeO_2 (JCPDS PDF 65–5923) and analogous

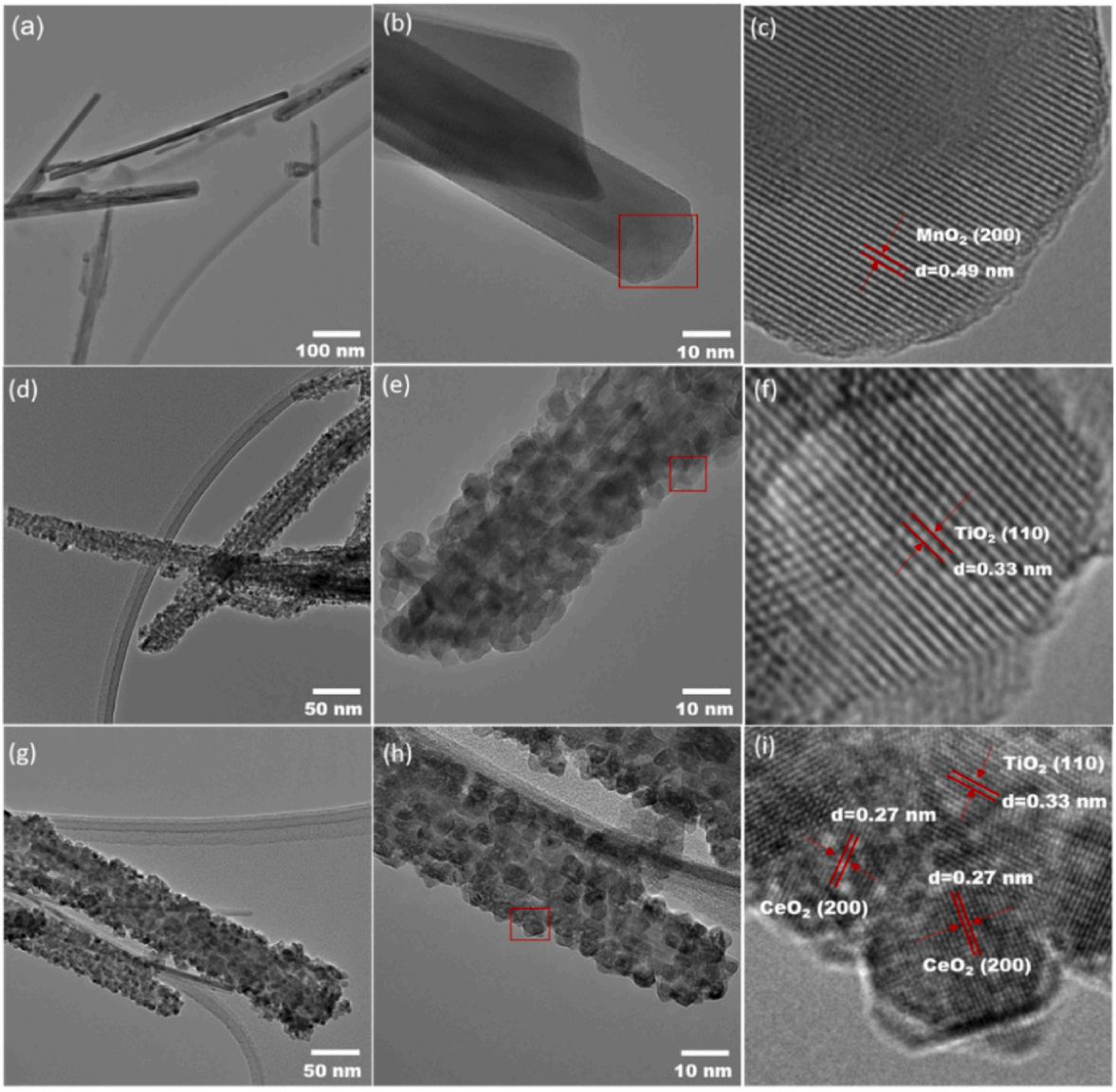

Fig. 6. TEM images of (a–c) MnO_x nanorods, (d–f) $MnO_x@TiO_2$ and (g–i) $MnO_x@TiO_2@CeO_2$ catalysts.

CeO_2 peaks were also present in $MnO_x@CeO_2$, while the crystalline MnO_2 phase in both catalysts were less obvious which was also the case after successive coating with TiO_2 in $MnO_x@CeO_2@TiO_2$.

The morphologies of MnO_x, $MnO_x@TiO_2$ and $MnO_x@TiO_2@CeO_2$ were examined by TEM (Fig. 6). The TEM images revealed that MnO_x had regular nanorod structure (Fig. 6a–c) with lattice fringes of 0.49 nm corresponding to the (200) crystal plane of MnO_2 (JCPDS PDF 72–1982). In addition, the kinetics-controlled coating process generated core-shell $MnO_x@TiO_2$ having MnO_x nanorods enclosed with TiO_2 nanoparticles (Fig. 6d–f) with distinctive lattice fringes of 0.33 nm matching the (110) crystal plane of TiO_2 (JCPDS PDF 48–1278). In the case of $MnO_x@TiO_2@CeO_2$, the TEM images (Fig. 6g–h) further confirmed that the $MnO_x@TiO_2@CeO_2$ maintained a core-shell structure with outer lattice fringes of 0.27 nm ascribed to the (200) plane of CeO_2 (JCPDS PDF 65–5923) and inner fringes of the (110) plane of TiO_2, indicating deposition of a CeO_2 layer on the outer surface of $MnO_x@TiO_2$. The spatial distribution of elements in $MnO_x@TiO_2@CeO_2$ was also measured by elemental mapping using EDS (Fig. 7), which confirmed that Ce species were mainly located in the outer layer of the material, while Ti species dominated in the middle layer and Mn species in the interior of the catalyst, thus verifying a core-shell-shell structure of $MnO_x@TiO_2@CeO_2$.

Nitrogen adsorption/desorption isotherms of MnO_x, $MnO_x@CeO_2$, $MnO_x@CeO_2@TiO_2$, $MnO_x@TiO_2$ and $MnO_x@TiO_2@CeO_2$ (Fig. S5) were typical type-IV isotherms with H3 hysteresis loops (IUPAC classification) demonstrating mesoporous structures. The specific surface areas, pore volumes and pore sizes of the catalysts are summarized in Table 1. Compared to the MnO_x nanorods, $MnO_x@TiO_2$ displayed a much higher specific surface area as well as pore volume likely due to high dispersion of TiO_2 on the surface of the nanorods in accordance with the result of XRD, while only marginally differences were found for $MnO_x@CeO_2$. After coating with additional layers of CeO_2 or TiO_2, the specific surface of both catalysts decreased slightly, however, $MnO_x@TiO_2@CeO_2$ retained a relatively higher specific surface area (64.3 m^2/g) than $MnO_x@CeO_2@TiO_2$ (49.5 m^2/g). The higher specific surface is expected to provide more active sites, which likely played an important role for its better NH_3-SCR performance.

3.2.2. *Composition*

To determine surface chemical compositions and elemental states were XPS measurements carried out with MnO_x, $MnO_x@TiO_2$ and $MnO_x@TiO_2@CeO_2$. The Mn 2p spectra (Fig. 8a) had two main peaks

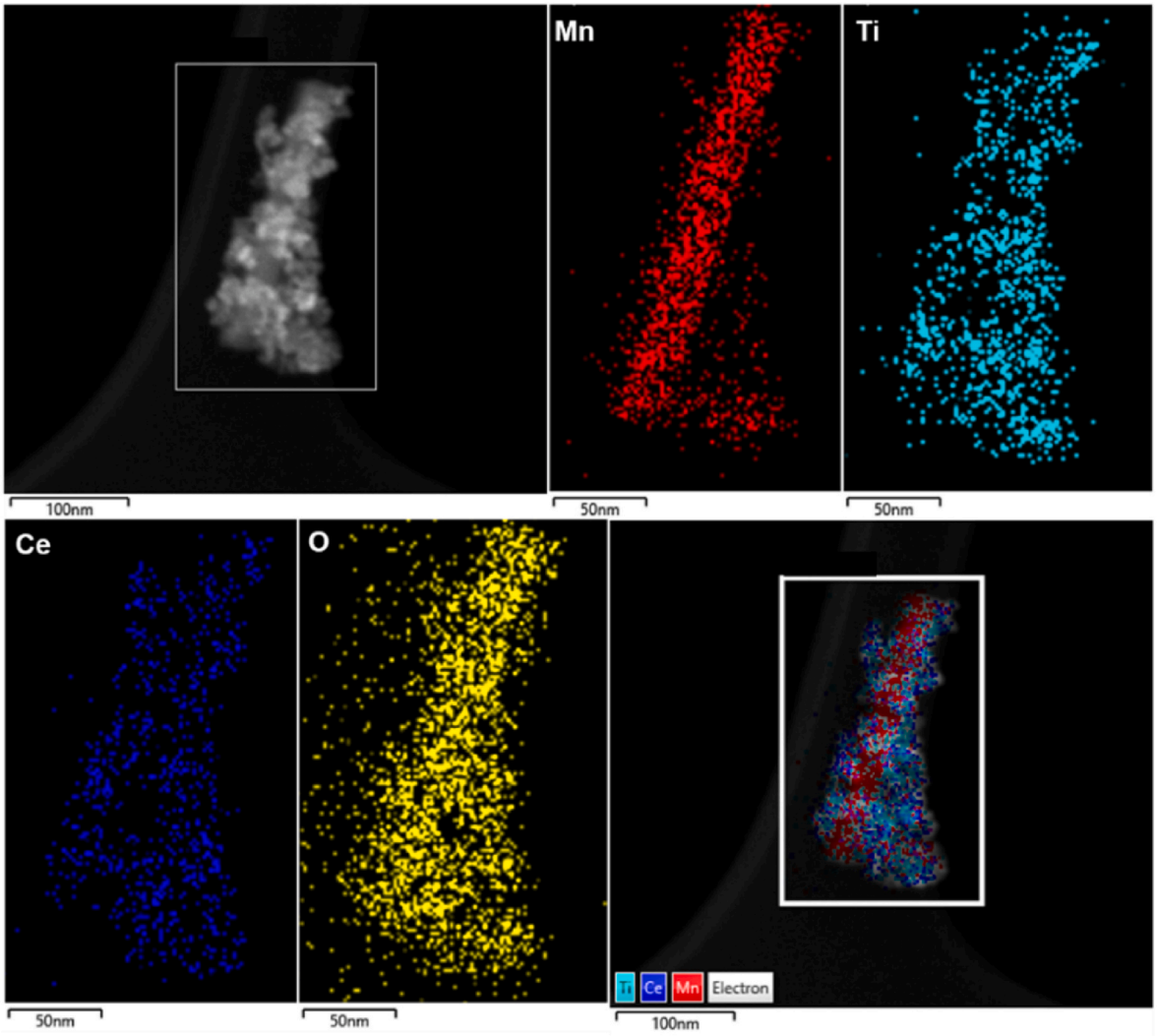

Fig. 7. TEM EDS elemental mapping images of MnO_x@TiO_2@CeO_2 catalyst.

Table 1
Specific surface area, pore volume and average pore size of catalysts.[a]

Catalyst	Surface area (m^2/g)	Pore volume (cm^3/g)	Average pore size (nm)
MnO_x	45.0	0.12	10.98
MnO_x@CeO_2	50.4	0.09	7.37
MnO_x@CeO_2@TiO_2	49.5	0.10	8.44
MnO_x@TiO_2	67.2	0.14	8.58
MnO_x@TiO_2@CeO_2	64.3	0.13	8.27

[a] Determined by N_2 adsorption/desorption.

around 644 and 654 eV attributed to Mn $2p_{3/2}$ and Mn $2p_{1/2}$ [37,38], where the former peak could be deconvoluted into separate peaks of Mn^{3+} (642.7 eV) and Mn^{4+} (645.8 eV) [39]. The relative atomic ratio of Mn^{4+} compared to Mn^{3+} was calculated from integrated peak areas as $Mn^{4+}/(Mn^{4+} + Mn^{3+})$ to be 15.2, 28.1 and 28.6% for MnO_x, MnO_x@TiO_2 and MnO_x@TiO_2@CeO_2, respectively (Table 2), thus indicating that the coating of TiO_2 resulted in a significant increase of Mn^{4+} on the MnO_x@TiO_2 and MnO_x@TiO_2@CeO_2 catalysts. The generation of more surface Mn^{4+} could be due to strong interaction occurring through the interface between the MnO_x and TiO_2 layers, which facilitates charge transfer between Mn and Ti as demonstrated previously in the literature [35,40–42]. The higher Mn^{4+} ratios were likely propitious to their LT NH_3-SCR performance as also demonstrated previously for other Mn-based catalysts [37,43]. Notably, as expected the Mn 2p signals obtained with MnO_x@TiO_2 and MnO_x@TiO_2@CeO_2 were also less intense indicating a lower Mn concentration in the outer surface of the core-shell materials. In line with this, XRF analyses of the two core-shell catalysts showed higher Mn/Ti and Mn/Ce bulk atomic ratios than the corresponding atomic surface ratios determined by XPS. Overall, the results corroborated that Ce was mainly located in the outer layer, Ti in the middle layer and Mn in the interior of the MnO_x@TiO_2@CeO_2 catalyst, which matched very well with the TEM EDS results.

The O 1s XPS spectra of the three catalysts were also recorded (Fig. 8b) and could be deconvoluted into two peaks O_α (529.7 eV) and O_β (531.8 eV) assigned to lattice oxygen and chemisorbed oxygen, respectively [44–46]. The ratio of O_β was calculated by the integral areas of $O_\beta/(O_\beta + O_\alpha)$ (Table 2) and showed that MnO_x@TiO_2 and MnO_x@TiO_2@CeO_2 had much higher O_β ratio than MnO_x. In general, electrophilic O_β with high mobility is more reactive and more easily exchanged with gas oxygen or oxygen molecules adsorbed on a catalyst surface in comparison to O_α [47–49], thus suggesting that the higher O_β concentration likely also contributed to the improved catalytic performance found for MnO_x@TiO_2 and MnO_x@TiO_2@CeO_2 in the NH_3-SCR reaction.

3.2.3. *Acidity and redox properties*

H_2-TPR experiments were conducted with the MnO_x, MnO_x@TiO_2 and MnO_x@TiO_2@CeO_2 catalysts (Fig. 9) to probe the redox properties

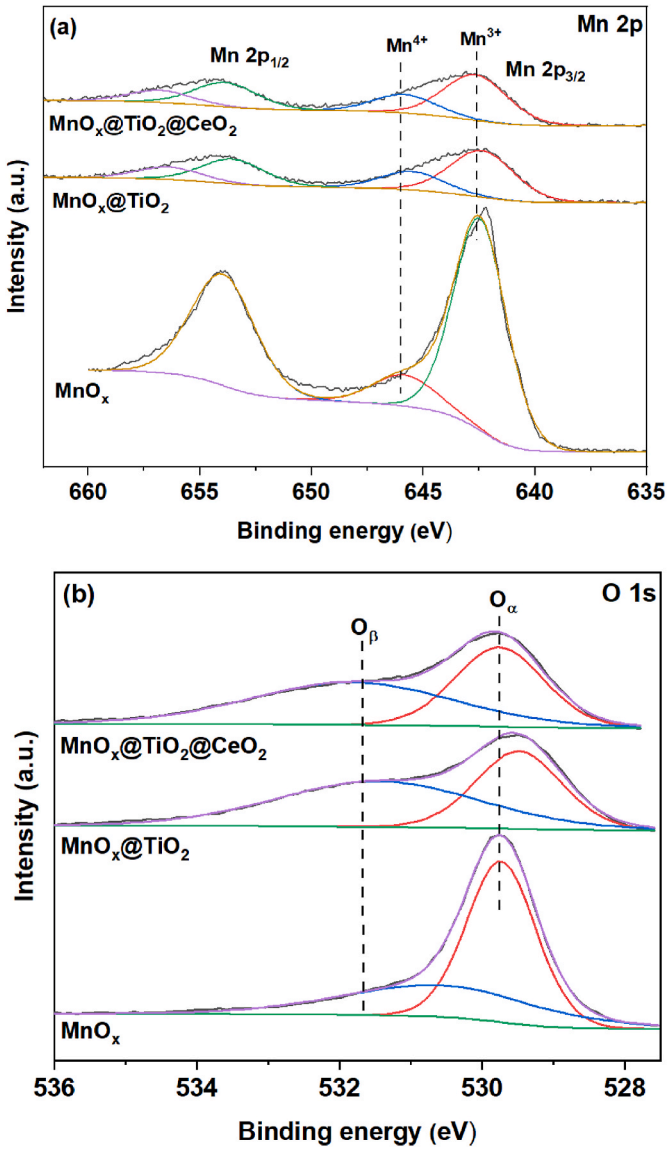

Fig. 8. XPS spectra of (a) Mn 2p and (b) O 1s of MnO_x, $MnO_x@TiO_2$ and $MnO_x@TiO_2@CeO_2$.

of MnO_x, which according to literature is reduced stepwise (i.e., $MnO_2 \rightarrow Mn_2O_3 \rightarrow Mn_3O_4 \rightarrow MnO$) between 150 and 500 °C [37,50,51]. Pristine MnO_x only had one broad and strong reduction band centered at 343 °C, which probably comprised overlapping peaks of the different reduction steps. Such excessive number of redox sites on the catalyst might have facilitated the unselective oxidation of NH_3 and poor SCR performance experienced at higher temperatures of 200–300 °C. Oppositely, both $MnO_x@TiO_2$ and $MnO_x@TiO_2@CeO_2$ exhibited three distinct reduction peaks around 290, 340 and 480 °C attributed to the sequential reduction steps. Notably, the additional CeO_2 coating had minor influence on the redox property as both peak intensities and positions remained rather similar for the core-shell catalysts.

Catalyst surface acidity also plays an important role for the performance in NH_3-SCR [52,53] and the acidities of MnO_x, $MnO_x@TiO_2$ and $MnO_x@TiO_2@CeO_2$ were therefore further evaluated by NH_3-TPD (Fig. 10). MnO_x exhibited a broad peak in the range of 100–200 °C attributed to weak acid sites, while an intense peak >525 °C likely originated from decomposition of the metal oxide as shown by supporting TG analysis (inset in Fig. 10). For $MnO_x@TiO_2$ and $MnO_x@TiO_2@CeO_2$ additional broad peaks appearing at 200–300 °C suggested that the coating shells induced more medium acid sites especially for the latter double-layered catalyst. Moreover, new peaks around 500 °C for the latter catalysts attributed to the release of oxygen from the decomposition of MnO_2 to Mn_2O_3 [54,55], indicated that these catalysts contained more surface Mn^{4+} than MnO_x in accordance with the results from the Mn 2p XPS. Thus, overall the abundant acid sites in $MnO_x@TiO_2@CeO_2$ contributed not only to improve the LT SCR activity of the catalyst, but it also beneficially affected its water resistance by alleviating the inhibiting effect of water due to competitive adsorption with NH_3 on acid sites [56–58].

4. Conclusions

The syntheses of highly active and durable LT NH_3-SCR catalysts is imperative for NO_x control in industrial processes. In this regard, the rational design of core-shell catalysts has attracted significant attention due to their unique structure properties. In this work, MnO_x nanorod and derived core-shell catalysts with TiO_2 and CeO_2 were prepared, characterized and their performance for LT NH_3-SCR studied under different conditions. The core-shell-shell $MnO_x@TiO_2@CeO_2$ catalyst displayed

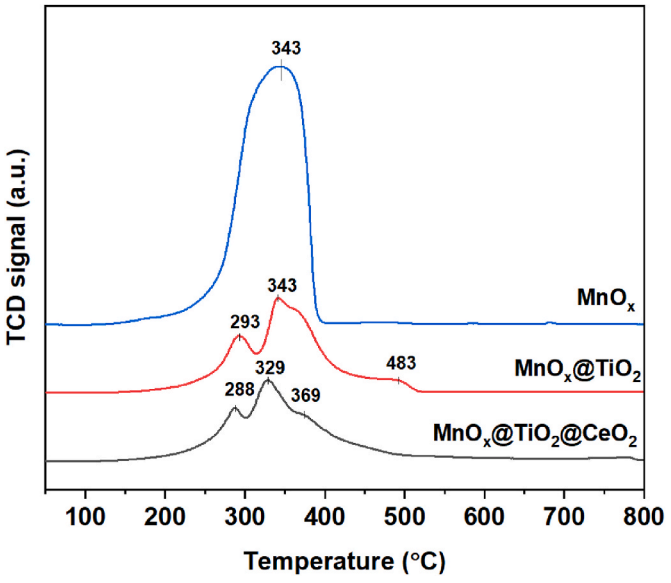

Fig. 9. H_2-TPR profiles of MnO_x, $MnO_x@TiO_2$ and $MnO_x@TiO_2@CeO_2$ catalysts.

Table 2
Composition of MnO_x, $MnO_x@TiO_2$, and $MnO_x@TiO_2@CeO_2$ catalysts.

Catalyst	Atomic concentration (%)							Relative atomic ratio (%)			
	XRF			XPS							
	Mn	Ti	Ce	Mn	Ti	Ce	O	Mn^{4+}	Mn^{3+}	O_α	O_β
MnO_x	100.0	0.0	0.0	31.3	0.0	0.0	63.6	15.2	84.8	64.1	35.9
$MnO_x@TiO_2$	87.9	12.1	0.0	15.0	15.5	0.0	61.4	28.1	71.9	41.9	58.1
$MnO_x@TiO_2@CeO_2$	59.2	7.9	32.9	11.8	7.6	10.7	69.9	28.6	71.4	44.8	55.3

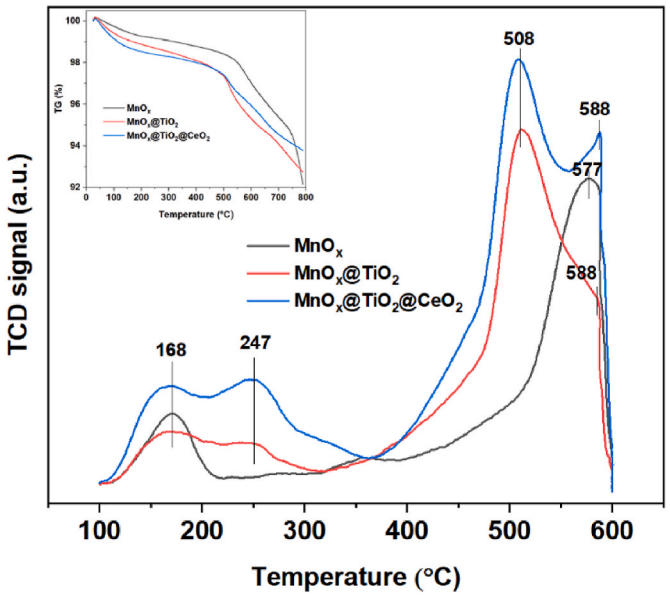

Fig. 10. NH_3-TPD and TG patterns (inset) of MnO_x, MnO_x@TiO_2 and MnO_x@TiO_2@CeO_2 catalysts.

excellent LT activity with NO_x conversion >80% in the temperature range 120–260 °C with dry feed gas and 180–255 °C with humid feed gas (2.5 vol% H_2O) using high WHSV of 240,000 mL/(g·h). Notably, the NO_x conversion remained also relatively high with more water in the feed gas (10 vol% H_2O), whereas water inhibition was much more pronounced with MnO_x nanorod and MnO_x@TiO_2 catalysts.

The XRD and TEM results provided clear evidence of the successful synthesis of the core-shell-shell MnO_x@TiO_2@CeO_2 catalyst. The highly dispersed TiO_2 nanoparticles formed an inner surface shell around the MnO_x nanorods, while CeO_2 nanoparticles formed the outer surface shell. BET results showed that the specific surface area of the catalyst increased significantly due to the presence of the evenly distributed TiO_2 shell. The high surface area could enhance the accessibility of the active sites, leading to improved catalytic activity. In addition, the XPS results revealed that the TiO_2 shell also markedly increased the surface Mn^{4+} ratio and chemisorbed oxygen, which was likely due to the strong interaction occurring through the interface between the TiO_2 shell and MnO_x nanorods. Mn^{4+} is demonstrated to be the main active species responsible for the oxidation of NO to NO_2, and the presence of chemisorbed oxygen could facilitate this reaction, thus promoting the LT NH_3-SCR activity. Furthermore, the NH_3-TPD results indicated that the outer CeO_2 shell significantly increased the acid density of MnO_x@TiO_2@CeO_2, which was beneficial for NH_3 adsorption. NH_3 adsorption is a crucial step for the SCR reaction to proceed. The increased acid density could also alleviate the competitive adsorption between NH_3 and water, contributing to the enhanced water tolerance, which is essential for the durability of the catalyst under practical operating conditions.

Overall, the inner TiO_2 and outer CeO_2 shells have been shown to play important roles in improving the specific surface area, surface Mn^{4+} ratio, chemisorbed oxygen and acid density, leading to excellent LT activity and good water tolerance. The work demonstrates that rational core-shell catalyst design can lead to high LT performance as well as improved durability of Mn-based NH_3-SCR catalysts.

Declaration of competing interest

The authors declare that they have no known competing financial interests or personal relationships that could have appeared to influence the work reported in this paper.

Acknowledgements

H.L. thanks the China Scholarship Council (No. 202004910329) for awarding a scholarship and the Department of Chemistry, Technical University of Denmark is acknowledged for supporting the work.

Appendix A. Supplementary data

Supplementary data to this article can be found online at https://doi.org/10.1016/j.joei.2023.101266.

References

[1] B. Guan, R. Zhan, H. Lin, Z. Huang, Review of state of the art technologies of selective catalytic reduction of NO_x from diesel engine exhaust, Appl. Therm. Eng. 66 (2014) 395–414.
[2] R.Y. Xie, L. Ma, Z.H. Li, Z. Qu, N.Q. Yan, J.H. Li, Review of sulfur promotion effects on metal oxide catalysts for NO_x emission control, ACS Catal. 11 (2021) 13119–13139.
[3] S. Roy, M. Hegde, G. Madras, Catalysis for NO_x abatement, Appl. Energy 86 (2009) 2283–2297.
[4] H. Bosch, F. Janssen, Catalytic reduction of nitrogen oxides: a review on the fundamentals and technology, Catal. Today 2 (1988) 369–531.
[5] M. Radojevic, Reduction of nitrogen oxides in flue gases, Environ. Pollut. 102 (1998) 685–689.
[6] F. Gholami, M. Tomas, Z. Gholami, M. Vakili, Technologies for the nitrogen oxides reduction from flue gas: a review, Sci. Total Environ. (2020), 136712.
[7] L. Lietti, G. Ramis, F. Berti, G. Toledo, D. Robba, G. Busca, P. Forzatti, Chemical, structural and mechanistic aspects on NO_x SCR over commercial and model oxide catalysts, Catal. Today 42 (1998) 101–116.
[8] L.J. Alemany, L. Lietti, N. Ferlazzo, P. Forzatti, G. Busca, E. Giamello, F. Bregani, Reactivity and physicochemical characterization of V_2O_5-WO_3/TiO_2 de-NO_x catalysts, J. Catal. 155 (1995) 117–130.
[9] L. Lietti, I. Nova, G. Ramis, L. Dall'Acqua, G. Busca, E. Giamello, P. Forzatti, F. Bregani, Characterization and reactivity of V_2O_5-MoO_3/TiO_2 de-NO_x SCR catalysts, J. Catal. 187 (1999) 419–435.
[10] Y.J. Zheng, A.D. Jensen, J.E. Johnsson, Deactivation of V_2O_5-WO_3-TiO_2 SCR catalyst at a biomass-fired combined heat and power plant, Appl. Catal. B Environ. 60 (2005) 253–264.
[11] L. Chen, J. Li, M. Ge, Promotional effect of Ce-doped V_2O_5-WO_3/TiO_2 with low vanadium loadings for selective catalytic reduction of NO_x by NH_3, J. Phys. Chem. C 113 (2009) 21177–21184.
[12] M.H. Kim, S.-W. Ham, Determination of N_2O emissions levels in the selective reduction of NO_x by NH_3 over an on-site-used commercial V_2O_5-WO_3/TiO_2 catalyst using a modified gas cell, Top. Catal. 53 (2010) 597–607.
[13] C. Liu, J.W. Shi, C. Gao, C.M. Niu, Manganese oxide-based catalysts for low-temperature selective catalytic reduction of NO_x with NH_3: a review, Appl. Catal., A 522 (2016) 54–69.
[14] F.Y. Gao, X.L. Tang, H.H. Yi, S.Z. Zhao, C.L. Li, J.Y. Li, Y.R. Shi, X.M. Meng, A review on selective catalytic reduction of NO_x by NH_3 over Mn-based catalysts at low temperatures: catalysts, mechanisms, kinetics and DFT calculations, Catalysts 7 (2017) 199.
[15] S. Zhang, B. Zhang, B. Liu, S. Sun, A review of Mn-containing oxide catalysts for low temperature selective catalytic reduction of NO_x with NH_3: reaction mechanism and catalyst deactivation, RSC Adv. 7 (2017) 26226–26242.
[16] G.Y. Xu, X.L. Guo, X.X. Cheng, J. Yu, B.Z. Fang, A review of Mn-based catalysts for low-temperature NH_3-SCR: NO_x removal and H_2O/SO_2 resistance, Nanoscale 13 (2021) 7052–7080.
[17] X. Zhou, F. Yu, R.B. Sun, J.Q. Tian, Q. Wang, B. Dai, J.M. Dan, H. Pfeiffer, Two-dimensional MnFeCo layered double oxide as catalyst for enhanced selective catalytic reduction of NO_x with NH_3 at low temperature (25-150 °C), Appl. Catal. A Gen. 592 (2020), 117432.
[18] N.Q. Zhang, L.C. Li, Y.Z. Guo, J.D. He, R. Wu, L.Y. Song, G.Z. Zhang, J.S. Zhao, D. S. Wang, H. He, A MnO_2-based catalyst with H_2O resistance for NH_3-SCR: study of catalytic activity and reactants-H_2O competitive adsorption, Appl. Catal. B Environ. 270 (2020) 14.
[19] G. Gao, J.-W. Shi, Z. Fan, C. Gao, C. Niu, MnM_2O_4 microspheres (M = Co, Cu, Ni) for selective catalytic reduction of NO with NH_3: comparative study on catalytic activity and reaction mechanism via in-situ diffuse reflectance infrared Fourier transform spectroscopy, Chem. Eng. J. 325 (2017) 91–100.
[20] Z.Y. Fan, J.W. Shi, C.H. Niu, B.R. Wang, C. He, Y.H. Cheng, The insight into the role of Al_2O_3 in promoting the SO_2 tolerance of MnO_x for low-temperature selective catalytic reduction of NO_x with NH_3, Chem. Eng. J. (2020) 398.
[21] Z. Jiang, Q. Wang, Y. Cai, Enhanced catalytic activity and SO_2/H_2O tolerance for selective catalytic reduction of NO_x with NH_3 over titanate nanotubes supported MnO_x-CeO_2 catalyst at low temperature, Catal. Surv. Asia 26 (2022) 161–173.
[22] X.B. Wang, S.G. Wu, W.X. Zou, S.H. Yu, K.T. Gui, L. Dong, Fe-Mn/Al_2O_3 catalysts for low temperature selective catalytic reduction of NO with NH_3, Chin. J. Catal. 37 (2016) 1314–1323.
[23] S. Raja, M.S. Alphin, L. Sivachandiran, Promotional effects of modified TiO_2- and carbon-supported V_2O_5- and MnO_x-based catalysts for the selective catalytic reduction of NO_x: a review, Catal. Sci. Technol. 10 (2020) 7795–7813.

[24] S. Xiong, Y. Liao, X. Xiao, H. Dang, S. Yang, The mechanism of the effect of H_2O on the low temperature selective catalytic reduction of NO with NH_3 over Mn-Fe spinel, Catal. Sci. Technol. 5 (2015) 2132–2140.

[25] S. Yang, F. Qi, S. Xiong, H. Dang, Y. Liao, P.K. Wong, J. Li, MnO_x supported on Fe-Ti spinel: a novel Mn based low temperature SCR catalyst with a high N_2 selectivity, Appl. Catal. B Environ. 181 (2016) 570–580.

[26] N.Q. Zhang, H. He, D.S. Wang, Y.D. Li, Challenges and opportunities for manganese oxides in low-temperature selective catalytic reduction of NO_x with NH_3: H_2O resistance ability, J. Solid State Chem. 289 (2020) 9.

[27] R. Ghosh Chaudhuri, S. Paria, Core/shell nanoparticles: classes, properties, synthesis mechanisms, characterization, and applications, Chem. Rev. 112 (2012) 2373–2433.

[28] M.B. Gawande, A. Goswami, T. Asefa, H.Z. Guo, A.V. Biradar, D.L. Peng, R. Zboril, R.S. Varma, Core-shell nanoparticles: synthesis and applications in catalysis and electrocatalysis, Chem. Soc. Rev. 44 (2015) 7540–7590.

[29] X.Y. Zhang, H. Wang, X. Jiang, H.C. Sun, Z.P. Qu, Study of synergistic effect between CuO and CeO_2 over CuO@CeO_2 core-shell nanocomposites for NH_3-SCO, Catal. Sci. Technol. 9 (2019) 2968–2981.

[30] D.R. Ma, L. Yang, B.J. Huang, L.T. Wang, X. Wang, Z.Y. Sheng, F. Dong, MnO_x-CeO_2@TiO_2 core-shell composites for low temperature SCR of NO_x, New J. Chem. 43 (2019) 15161–15168.

[31] A.K. Datye, M. Votsmeier, Opportunities and challenges in the development of advanced materials for emission control catalysts, Nat. Mater. 20 (2021) 1049–1059.

[32] Z.Y. Sheng, D.R. Ma, D.Q. Yu, X. Xiao, B.J. Huang, L. Yang, S. Wang, Synthesis of novel MnO_x@TiO_2 core-shell nanorod catalyst for low-temperature NH_3-selective catalytic reduction of NO_x with enhanced SO_2 tolerance, Chin. J. Catal. 39 (2018) 821–830.

[33] C.Y. Huang, R.T. Guo, W.G. Pan, X. Sun, S.W. Liu, J. Liu, Z.Y. Wang, X. Shi, SCR of NO_x by NH_3 over $MnFeO_x$@TiO_2 catalyst with a core-shell structure: the improved K resistance, J. Energy Inst. 92 (2019) 1364–1378.

[34] C.L. Yu, D. Hou, B.C. Huang, M.J. Lu, R.S. Peng, Z.Y. Zhong, A MnO_x@Eu-CeO_x nanorod catalyst with multiple protective effects: strong SO_2-tolerance for low temperature deNO_x processes, J. Hazard Mater. 399 (2020), 123011.

[35] X.S. Huang, F. Dong, G.D. Zhang, Y. Guo, Z.C. Tang, A strategy for constructing highly efficient yolk-shell Ce@Mn@TiO_x catalyst with dual active sites for low-temperature selective catalytic reduction of NO with NH_3, Chem. Eng. J. 419 (2021) 13.

[36] W. Li, J. Yang, Z. Wu, J. Wang, B. Li, S. Feng, Y. Deng, F. Zhang, D. Zhao, A versatile kinetics-controlled coating method to construct uniform porous TiO_2 shells for multifunctional core–shell structures, J. Am. Chem. Soc. 134 (2012) 11864–11867.

[37] R.T. Guo, X. Sun, J. Liu, W.G. Pan, M.Y. Li, S.M. Liu, P. Sun, S.W. Liu, Enhancement of the NH_3-SCR catalytic activity of $MnTiO_x$ catalyst by the introduction of Sb, Appl. Catal., A Gen. 558 (2018) 1–8.

[38] R.T. Guo, S.X. Wang, W.G. Pan, M.Y. Li, P. Sun, S.M. Liu, X. Sun, S.W. Liu, J. Liu, Different poisoning effects of K and Mg on the Mn/TiO_2 catalyst for selective catalytic reduction of NO_x with NH_3: a mechanistic study, J. Phys. Chem. C 121 (2017) 7881–7891.

[39] Q.H. Yan, S.N. Chen, C. Zhang, Q. Wang, B. Louis, Synthesis and catalytic performance of $Cu_1Mn_{0.5}Ti_{0.5}O_x$ mixed oxide as low-temperature NH_3-SCR catalyst with enhanced SO_2 resistance, Appl. Catal. B Environ. 238 (2018) 236–247.

[40] Z. Fu, G. Zhang, W. Han, Z. Tang, The water resistance enhanced strategy of Mn based SCR catalyst by construction of TiO_2 shell and superhydrophobic coating, Chem. Eng. J. 426 (2021), 131334.

[41] Z. Cai, G. Zhang, Z. Tang, J. Zhang, $MnFeO_x$@TiO_2 nanocages for selective catalytic reduction of NO with NH_3 at low temperature, ACS Appl. Nano Mater. 4 (2021) 6201–6211.

[42] X. Huang, F. Dong, G. Zhang, Z. Tang, Constructing TiO_2@$CeMnO_x$ nanocages by self-sacrificial hydrolytic etching MIL-125 for efficient wide-temperature selective catalytic reduction of nitrogen oxides, Chem. Eng. J. 432 (2022), 134236.

[43] Z. Cai, G. Zhang, Z. Tang, J. Zhang, MnFe@CeO_x core-shell nanocages for the selective catalytic reduction of NO with NH_3 at low temperature, ACS Appl. Nano Mater. 5 (2022) 3619–3631.

[44] Y. Peng, J.H. Li, W.B. Shi, J.Y. Xu, J.M. Hao, Design strategies for development of SCR catalyst: improvement of alkali poisoning resistance and novel regeneration method, Environ. Sci. Technol. 46 (2012) 12623–12629.

[45] W. Hu, X. Gao, Y. Deng, R. Qu, C. Zheng, X. Zhu, K. Cen, Deactivation mechanism of arsenic and resistance effect of SO_4^{2-} on commercial catalysts for selective catalytic reduction of NO_x with NH_3, Chem. Eng. J. 293 (2016) 118–128.

[46] B. Zhang, M. Liebau, B. Liu, L. Li, S. Zhang, R. Gläser, Selective catalytic reduction of NO_x with NH_3 over Mn-Zr-Ti mixed oxide catalysts, J. Mater. Sci. 54 (2019) 6943–6960.

[47] P. Sun, R.T. Guo, S.M. Liu, S.X. Wang, W.G. Pan, M.Y. Li, The enhanced performance of MnO_x catalyst for NH_3-SCR reaction by the modification with Eu, Appl. Catal. A Gen. 531 (2017) 129–138.

[48] X. Fang, Y.J. Liu, Y. Cheng, W.L. Cen, Mechanism of Ce-modified birnessite-MnO_2 in promoting SO_2 poisoning resistance for low-temperature NH_3-SCR, ACS Catal. 11 (2021) 4125–4135.

[49] L. Chen, C. Zhang, Y.X. Li, C.R. Chang, C. He, Q. Lu, Y.S. Yu, P.G. Duan, Z.X. Zhang, R. Luque, Hierarchically hollow MnO_2@CeO_2 heterostructures for NO oxidation: remarkably promoted activity and SO_2 tolerance, ACS Catal. 11 (2021) 10988–10996.

[50] L.N. Gan, K.Z. Li, W.N. Yang, J.J. Chen, Y. Peng, J.H. Li, Core-shell-like structured alpha-MnO_2@CeO_2 catalyst for selective catalytic reduction of NO: promoted activity and SO_2 tolerance, Chem. Eng. J. 391 (2020) 8.

[51] R. Yan, S.X. Lin, Y.L. Li, W.M. Liu, Y.Y. Mi, C.J. Tang, L. Wang, P. Wu, H.G. Peng, Novel shielding and synergy effects of Mn-Ce oxides confined in mesoporous zeolite for low temperature selective catalytic reduction of NO_x with enhanced SO_2/H_2O tolerance, J. Hazard Mater. 396 (2020) 11.

[52] J.M.G. Amores, V.S. Escribano, G. Ramis, G. Busca, An FT-IR study of ammonia adsorption and oxidation over anatase-supported metal oxides, Appl. Catal. B Environ. 13 (1997) 45–58.

[53] Z.P. Zhang, Y.Y. Li, P.P. Yang, Y.S. Li, C. Zhao, R.M. Li, Y.J. Zhu, Improved NH_3-SCR deNO_x activity and tolerance to H_2O & SO_2 at low temperature over the $Nb_mCu_{(0.1)-m}Ce_{0.9}O_x$ catalysts: role of acidity by niobium doping, Fuel 303 (2021), 121239.

[54] D. Fang, J. Xie, H. Hu, H. Yang, F. He, Z. Fu, Identification of MnO_x species and Mn valence states in MnO_x/TiO_2 catalysts for low temperature, SCR. Chem. Eng. J. 271 (2015) 23–30.

[55] J. Li, J. Chen, R. Ke, C. Luo, J. Hao, Effects of precursors on the surface Mn species and the activities for NO reduction over MnO_x/TiO_2 catalysts, Catal. Commun. 8 (2007) 1896–1900.

[56] G. Busca, L. Lietti, G. Ramis, F. Berti, Chemical and mechanistic aspects of the selective catalytic reduction of NO_x by ammonia over oxide catalysts: a review, Appl. Catal. B Environ. 18 (1998) 1–36.

[57] I. Nova, L. Lietti, E. Tronconi, P. Forzatti, Dynamics of SCR reaction over a TiO_2-supported vanadia-tungsta commercial catalyst, Catal. Today 60 (2000) 73–82.

[58] H.Z. Chang, X.Y. Chen, J.H. Li, L. Ma, C.Z. Wang, C.X. Liu, J.W. Schwank, J. M. Hao, Improvement of activity and SO_2 tolerance of Sn-modified MnO_x-CeO_2 catalysts for NH_3-SCR at low temperatures, Environ. Sci. Technol. 47 (2013) 5294–5301.